Rich Ground State Chemical Ordering in Nanoparticles: Exact Solution of a Model for Ag-Au Clusters

Larsen, Peter Mahler; Jacobsen, Karsten Wedel; Schiøtz, Jakob

Published in:
Physical Review Letters

Link to article, DOI:
10.1103/PhysRevLett.120.256101

Publication date:
2018

Document Version
Publisher's PDF, also known as Version of record

Rich Ground-State Chemical Ordering in Nanoparticles: Exact Solution of a Model for Ag-Au Clusters

Peter Mahler Larsen, Karsten Wedel Jacobsen, and Jakob Schiøtz*
Center for Atomic-scale Materials Design (CAMD), Department of Physics, Technical University of Denmark, 2800 Kongens Lyngby, Denmark

(Received 23 December 2017; published 18 June 2018)

We show that nanoparticles can have very rich ground-state chemical order. This is illustrated by determining the chemical ordering of Ag-Au 309-atom Mackay icosahedral nanoparticles. The energy of the nanoparticles is described using a cluster expansion model, and a mixed integer programming approach is used to find the exact ground-state configurations for all stoichiometries. The chemical ordering varies widely between the different stoichiometries and displays a rich zoo of structures with nontrivial ordering.

DOI: 10.1103/PhysRevLett.120.256101

Ever since the surprising discovery by Haruta *et al.* that gold is catalytically active in nanoparticulate form [1], there has been intense research into the catalytic properties of gold [2–6] and silver [7] nanoparticles, including bimetallic Ag-Au nanoparticles [8–10]. These particles also display interesting optical and plasmonic properties, see, e.g., the reviews by Feng *et al.* [11] and Boote *et al.* [12], and show promising medical applications [13].

The catalytic properties of a nanoparticle often depend critically on the detailed atomic configuration [14,15]. This is particularly important for bimetallic nanoparticles, which can preferentially exhibit one or the other material on the surface, and often can be designed in so-called core-shell structures with one of the metals as the catalytically active shell. It has been demonstrated that the ability to tailor materials that naturally form desirable atomic-scale structures may significantly enhance catalytic activity and/or selectivity towards the desired reaction [15].

It is thus important to be able to predict the shape and chemical ordering of nanoparticles [16,17]. This is, however, a difficult task both due to the difficulty of calculating the energy of a given configuration accurately and mostly due to the very large configurational space that one must sample. This is usually done with Monte Carlo–based techniques, such as genetic algorithms [18–20], simulated annealing [21], basin hopping [22], or minima hopping [23]. While all these methods can efficiently find configurations that are close to the global minimum, one cannot in principle know how close to the optimum the solutions are, nor can one know for sure if the global optimum has been found.

In this Letter, we address the relatively simple case of bimetallic Au-Ag nanoparticles with 309 atoms in the Mackay icosahedral form. This is one of the so-called "magic number" structures where the per-atom energy is particularly low, leading to a morphology that is very robust to changes in stoichiometry and chemical ordering. We therefore only consider the chemical ordering, keeping the morphology constant. Even in this case, the search space is so large that it is unlikely that the stochastic methods find the ground state, for example, there are 4.7×10^{91} possible chemical orderings of the $Ag_{154}Au_{155}$ cluster. We address this by describing the energy of the nanoparticle using a cluster expansion (CE) model [24] fitted to the semi-empirical effective medium theory (EMT) [25] potential. This allows us to use a mixed integer programming (MIP) [26,27] approach to provably find the chemical ordering of the ground-state configuration. Details about the method can be found in the section on the computational approach.

We find ground-state configurations displaying a rich zoo of ordered structures, where the sites exposed on the nanoparticle surface vary dramatically with varying chemical composition of the nanoparticle. The configurations are not intuitive ground states, fitting into none of the well-studied categories of core-shell, Janus, or phase mixing nanoparticles [28].

Results.—We have minimized the energy to find the optimal configuration of the nanoparticle at every composition between 0 and 309 Au atoms. The nanoparticle exhibits a surprisingly complex structural evolution, as shown in Fig. 1. Figure 2 shows the number of Au atoms in each shell as a function of composition. Quite noticeable is that no shell shows a monotonic increase in Au content. Here, the second shell is particularly illustrative, in that it increases in Au content from 18 Au atoms, but has zero Au content again at 104 Au atoms. A further example (not shown in Fig. 2) is the central atom, which is occupied by a Au atom at 13 and 309 Au atoms only.

Figure 3 shows the convex hull of the formation energy of the ground-state configurations at every composition. The formation energy of a configuration $\boldsymbol{\sigma}$ with fractional compositions x_{Ag} and x_{Au} is given by

$$E_f(\boldsymbol{\sigma}) = \frac{1}{309}\left[E(\boldsymbol{\sigma}) - x_{\mathrm{Ag}}E_{\mathrm{Ag}} - x_{\mathrm{Au}}E_{\mathrm{Au}}\right]. \quad (1)$$

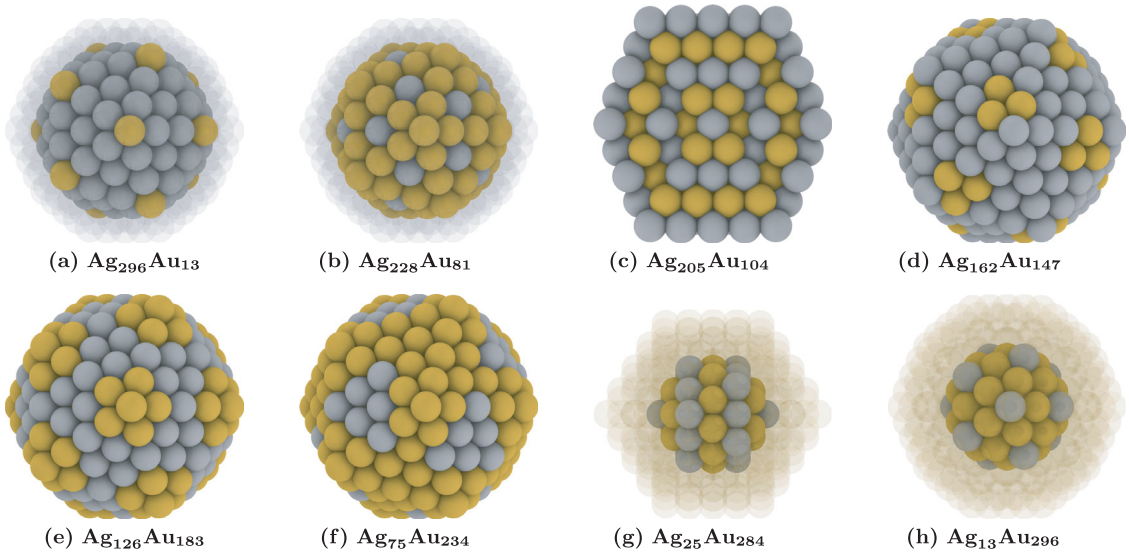

FIG. 1. A selection of ground-state configurations in a 309-atom Mackay icosahedron Ag-Au nanoparticle. The configurations exhibit a diverse range of highly ordered interior and surface structures. (a),(b) The transparent atoms represent a single layer of Ag atoms; (g),(h) they represent two layers of Au atoms. The Au atoms exhibit a strong preference for subsurface shell sites, in particular, the subsurface corners (a), followed by the subsurface edges (b). The Ag atoms show a strong preference for second shell corner sites (g),(h), as well as the central atom. The lowest energy configuration (c) (shown as a slice through the nanoparticle) has a perfectly ordered onion-shell structure. At high Au concentrations, the preference of Au atoms for corner, edge, or interior sites of the surface facets varies as a function of composition (d)–(f).

The convex hull contains a high number of compositions (99), which causes it to be a largely smooth function of composition. As such, the compositions highlighted are those where the energy gradient changes rapidly. These configurations (shown in Fig. 1) are remarkable in that they exhibit strong ordering, either rotationally symmetric ordering [Figs. 1(a)–1(c), 1(g), and 1(h)], or ordered geometric patterns [Figs. 1(d)–1(f)].

In many cases, regular patterns are formed inside the nanoparticle. Of particular interest is the $Ag_{205}Au_{104}$ cluster shown in Fig. 1(c), which forms an onionlike structure with alternating layers of pure Ag and Au. This structure has perfect icosahedral symmetry and is also the cluster with the most negative formation energy. A similar five-ring onion structure has been proposed by Cheng *et al.* [29] for Pd-Pt clusters, also using a semiempirical potential. The symmetric configurations at $Ag_{296}Au_{13}$ and $Ag_{13}Au_{296}$ [shown in Figs. 1(a) and 1(h), respectively] highlight the preference for occupation of subsurface corners for Au atoms, and second shell corners for Ag atoms.

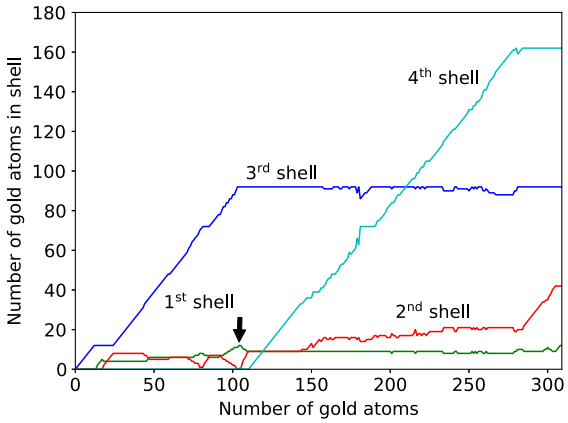

FIG. 2. Number of Au atoms in each shell vs the total number of Au atoms in the nanoparticle. The structural evolution exhibits a complex interplay between the shells, with no monotonically increasing shell occupancies.

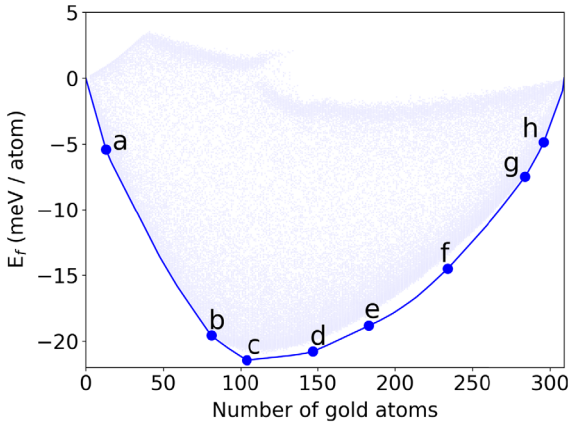

FIG. 3. Energy of formation (from EMT) vs the number of Au atoms in the nanoparticle. The gray dots show configurations sampled for CE model construction. The blue line shows the convex hull of the ground-state configurations. Compositions at which the nanoparticle exhibits strong ordering (shown in Fig. 1) are marked with a circle.

The flowerlike surface decoration shown in Fig. 1(e) is energetically favorable in the local concentration region. As can be seen in Fig. 2, the number of Au atoms in the fourth shell increases almost linearly in the range 110–284 Au atoms. However, there is a noticeable plateau in the region 181–190 Au atoms, where the flowers are present. Although the surface layer of the flower structure has icosahedral symmetry, the symmetry is broken in the interior layers.

From a graph theoretical perspective, the triangular Ag islands in the surface layer of the structure at 234 Au atoms [shown in Fig. 1(f)] exhibit a further peculiarity. Although the symmetry is broken (and one island is missing an atom), the eight islands fulfill the criteria of a maximum independent vertex set [30] in the dodecahedral platonic graph. This graph consists of 20 vertices (one for each facet of the nanoparticle) and 30 edges, which exist between adjacent facets. This means that no more than eight islands can be placed on the surface without overlap.

Other than strong geometric ordering, a characteristic of the structures is the change in preference for occupation of different site types as a function of concentration. For example, the nanoparticle in Fig. 1(d) shows how Au atoms form three-atom islands next to but not at the corners of the icosahedron. When the Au content is increased, however, the Au forms islands that switch to being centered on the corners [Fig. 1(e)]. Similarly, Ag atoms disfavor subsurface corners [Fig. 1(a)], but partially occupy these sites when the flower structures are present in the surface layer; this effect is shown in Fig. 2 by the dip in third shell occupation, which accompanies the plateau in the fourth shell (again, in the region 181–190 Au atoms).

All nanoparticles with up to 111 Au atoms only present Ag atoms in the surface, and all particles with more than 282 Au atoms only present Au atoms in the surface, in spite of the lower surface energy of Ag. This is contrary to the results of studies of other bimetallic nanoparticles in which the driving force of surface segregation is the relative surface energies [31]. Instead, the driving force [32] of the structural evolution as a function of composition is a trade-off between the large energetic differences between site types (shown in Fig. 4) and a preference for Ag and Au to form heteroatomic bonds, which in bulk materials at 0 K results in the formation of ordered alloys (see also Supplemental Material, Sec. S1 [33]).

To a first approximation, ground-state configurations are stable at moderate temperatures if the first excited state differs in the site-occupancy or nearest-neighbor coordination statistics. At a majority of concentrations, the density of low-energy states is high. Nonetheless, we have identified more than 10 ground-state structures where the energy gap to the first excited state is in the range 10–30 meV (see Supplemental Material, Sec. S2 [33]); this suggests that production and observation of some of these structures should, in principle, be possible in a moderately cooled laboratory setting.

The remarkably rich chemical ordering has been obtained despite the use of a relatively simple semiempirical potential, with no angular-dependent terms and a significantly lower complexity than a full *ab initio* Hamiltonian. We note that, regardless of the energetic model used, Monte Carlo methods are incapable of determining the optimality of a configuration; the conclusions of the present work rely on the ability of the MIP model to guarantee that the structures found are indeed the ground-state structures of the CE model.

The nanoparticle ground-state structures can viewed online at the Computational Materials Repository [34].

Computational approach.—Given a fixed site geometry, a cluster expansion uses pseudospin variables at each site in conjunction with an orthogonal basis (the clusters) to model configurational properties of the system. Specifically, a cluster Hamiltonian is of the form

$$E(\boldsymbol{\sigma}) = V_0 + \sum_{i\in\mathbf{C}_1} V_i^{(1)}\sigma_i + \sum_{(i,j)\in\mathbf{C}_2} V_{i,j}^{(2)}\sigma_i\sigma_j + \sum_{(i,j,k)\in\mathbf{C}_3} V_{(i,j,k)}^{(3)}\sigma_i\sigma_j\sigma_k + \cdots, \tag{2}$$

where $E(\boldsymbol{\sigma})$ is the energy of a configuration $\boldsymbol{\sigma}$, $\mathbf{C}_n$ is the set of all n-body clusters, each containing cluster instances i, (i,j), or (i,j,k) for one-, two-, or three-atom clusters, respectively, collectively referred to as $\mathbf{c}_f$ in the following; $V_{\mathbf{c}_f}^{(n)}$ are the effective cluster interactions (ECIs) for the

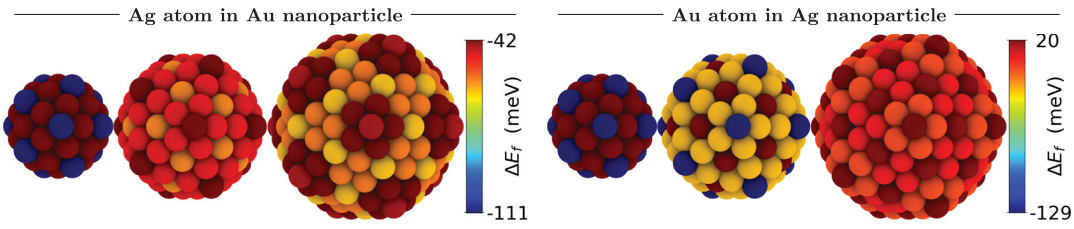

FIG. 4. Change in formation energy in pure nanoparticles upon the replacement of a single atom with the opposite species, for all sites in the outer three shells. This simple measure accounts for much of the variation in the ground-state structures, but is tempered at higher concentrations by a preference for heteroatomic bonding.

n-body cluster instances, and σ_i is the pseudospin variable at each site i.

A standard transformation is to change the spin variables $\sigma_i \in \{-1, 1\}$ to binary variables $x_i \in \{0, 1\}$ using the relation $\sigma_i = (2x_i - 1)$, which produces an equivalent Hamiltonian with different ECIs, but only binary variables. It can be written compactly as

$$E(\boldsymbol{x}) = E_0 + \sum_{\mathbf{c}_f} E_{\mathbf{c}_f} \prod_{i \in \mathbf{c}_f} x_i, \tag{3}$$

where $E_{\mathbf{c}_f}$ are the new ECIs. With a Hamiltonian in this form, we can formulate a MIP model in order to find provably optimal configurations. MIP models, which are a generalization of linear programming models, solve problems of the form

$$\text{minimize } \mathbf{c}^T\mathbf{x} \text{ (objective function)},$$
$$\text{subject to } \mathbf{A}\mathbf{x} \leq \mathbf{b} \text{ (constraints)}.$$

A linear program consists of a set of n continuous variables $\mathbf{x} \in \mathbb{R}^n$, an associated set of costs for each variable $\mathbf{c} \in \mathbb{R}^n$, and a set of m linear constraints, denoted here by $\mathbf{A} \in \mathbb{R}^{m \times n}$ and $\mathbf{b} \in \mathbb{R}^m$. The goal, or "objective function," is to find values for the set $\mathbf{x}$ such that the total cost is provably minimized, while respecting the constraints. In a MIP model, some or all of the variables are furthermore constrained to have integer values.

Table I shows the MIP model for determining the ground-state chemical ordering of a bimetallic nanoparticle. Each predetermined site, with index i, has an associated binary variable x_i (S1) which determines whether an A- or B-type atom is placed at that site. The system can (optionally) be constrained to contain N_B B-type atoms, using Eq. (S6). The activity of a cluster instance, indicated by a binary variable $y_{\mathbf{c}_f}$ (S2), is governed by Eqs. (S7) and (S8); taken together, these constraints are equivalent to the relation $y_{\mathbf{c}_f} = \prod_{i \in \mathbf{c}_f} x_i$. Finally, associated with each cluster is a predetermined ECI (S3) which is used to determine the total energy of the system (S5). Thus, the objective of the model is to choose how to order the A- and B-type atoms such that the total energy of the system is minimized.

In addition to ground-state configurations, a MIP model can be extended to find configurations of higher energy by adding linear constraints that forbid specific solutions, known as "set-covering constraints" [35]. Given a known ground-state configuration $\mathbf{x}'$, we can forbid it with the constraint

$$\sum_{i:x_i'=0} x_i + \sum_{i:x_i'=1} (1 - x_i) \geq 1. \tag{4}$$

Constraints of this form are added for all solutions that are symmetrically equivalent to $\mathbf{x}'$. When resolving the MIP model, the ground-state solution is now forbidden, and the lowest excited state is found instead.

The MIP method we apply is a widely used technique in applied mathematics, logistics, and industrial planning, but has not previously been used for the solution of ground states and excited states in a CE model. A different approach to finding provably optimal ground states was recently demonstrated by Huang *et al.* [36], making use of pseudo-Boolean optimization, rather than MIP, and applying it to bulk alloys.

Cluster selection and ECI fitting—For a system as large as a 309-atom nanoparticle, full electronic structure energy calculations are very time consuming. As such, sampling a sufficient number of configurations for a CE model is impractical. Instead, we use the semiempirical EMT [25] potential to calculate energies. Semiempirical potentials are fast to evaluate and highly accurate in bulk systems, but typically mispredict the energies of surface atoms. Nonetheless, while the energies might be quantitatively inaccurate, the different site types in a 309-atom nanoparticle have such great variation in energy that we can expect the energy difference of different configurations to be at least qualitatively correct.

To fit the ECI parameters, we have sampled 75 000 chemical ordering configurations at a range of high and low energies (cf. Fig. 3). The energy of each configuration has been minimized using gradient descent to allow local

TABLE I. A MIP model for determining the configuration that provably minimizes the energy of a CE model. The placement of the sites as well as the ECIs are fixed; the model determines the optimal chemical ordering only. For any cluster instance with a positive (negative) ECI, the constraint given by Eq. (S7) [Eq. (S8)] is redundant.

Variables:	$x_i \in \{0, 1\}$	$\forall i$ Type of atom site i ($A = 0$, $B = 1$)	(S1)
	$y_{\mathbf{c}_f} \in \{0, 1\}$	$\forall \mathbf{c}_f$ Cluster instance variable (off $= 0$, on $= 1$)	(S2)
Parameters:	$E_{\mathbf{C}} \in \mathbb{R}$	$\forall \mathbf{C}$ Energy of cluster $\mathbf{C}$	(S3)
	$N_B \in \mathbb{N}$	Number of B-type atoms	(S4)
Minimize:	$\sum_{\mathbf{C}} \sum_{\mathbf{c}_f \in \mathbf{C}} E_{\mathbf{C}} y_{\mathbf{c}_f}$	Total energy of system	(S5)
Subject to:	$\sum_i x_i = N_B$	Fixed number of B-type atoms	(S6)
	$y_{\mathbf{c}_f} \leq x_i$	$\forall i \in \mathbf{c}_f$ Any atom absent from $\mathbf{c}_f \Rightarrow y_{\mathbf{c}_f}$ off	(S7)
	$y_{\mathbf{c}_f} \geq 1 - \lvert\mathbf{c}_f\rvert + \sum_{i \in \mathbf{c}_f} x_i$	All atoms present in $\mathbf{c}_f \Rightarrow y_{\mathbf{c}_f}$ on	(S8)

relaxations without changing the overall structure of the nanoparticle. The constructed CE model, which contains 60 one-, two-, and three-body clusters, has a root-mean-square error of 0.060 meV/atom. Full details on the CE model can be found in the Supplemental Material, Sec. S3 [33].

The approach described here is not specific to 309-atom Mackay icosahedra—it generalizes well to other nanoparticle morphologies. A precondition for the use of a CE model, however, is the ability to identify a set of atomic sites. Given sufficient training data, the energetic effects of relaxations can be captured in the CE model, given that the relaxations are of limited magnitude and strictly local; i.e., they do not affect the neighbor relationships between atomic sites. While the solution time of a MIP model is dependent on many factors, our experience with the nanoparticle described here suggests that solving systems larger than a few hundred atoms is prohibitively expensive without reducing the number of clusters and thereby the accuracy of the CE model.

P. M. L. thanks John Connelly for productive discussions, Christopher Schuh for an introduction to the nanoparticle design problem, and Jesper Larsen for advice on selecting solver settings. This work was supported by research Grants No. 7026-00126B and No. 1335-00027B from the Danish Council for Independent Research and Grant No. 9455 from VILLUM FONDEN.

*schiotz@fysik.dtu.dk

[1] M. Haruta, T. Kobayashi, H. Sano, and N. Yamada, Chem. Lett. **16**, 405 (1987).
[2] M.-C. Daniel and D. Astruc, Chem. Rev. **104**, 293 (2004).
[3] T. Ishida, H. Koga, M. Okumura, and M. Haruta, Chem. Rec. **16**, 2278 (2016).
[4] R. Sardar, A. M. Funston, P. Mulvaney, and R. W. Murray, Langmuir **25**, 13840 (2009).
[5] M. Chen and D. W. Goodman, Acc. Chem. Res. **39**, 739 (2006).
[6] F. Gao, T. E. Wood, and D. W. Goodman, Catal. Lett. **134**, 9 (2010).
[7] J.-Z. Guo, H. Cui, W. Zhou, and W. Wang, J. Photochem. Photobiol. A **193**, 89 (2008).
[8] J.-H. Liu, A.-Q. Wang, Y.-S. Chi, H.-P. Lin, and C.-Y. Mou, J. Phys. Chem. B **109**, 40 (2005).
[9] C. M. Chang, C. Cheng, and C. M. Wei, J. Chem. Phys. **128**, 124710 (2008).
[10] P. Raveendran, J. Fu, and S. L. Wallen, Green Chem. **8**, 34 (2006).
[11] L. Feng, G. Gao, P. Huang, K. Wang, X. Wang, T. Luo, and C. Zhang, Nano BioMed. Eng. **2**, 258 (2010).
[12] B. W. Boote, H. Byun, and J.-H. Kim, J. Nanosci. Nanotechnol. **14**, 1563 (2014).
[13] M. Bachelet, Mater. Sci. Technol. **32**, 794 (2016).
[14] K. Honkala, A. Hellman, I. N. Remediakis, A. Logadottir, A. Carlsson, S. Dahl, C. H. Christensen, and J. K. Nørskov, Science **307**, 555 (2005).
[15] S. Siahrostami, A. Verdaguer-Casadevall, M. Karamad, D. Deiana, P. Malacrida, B. Wickman, M. Escudero-Escribano, E. A. Paoli, R. Frydendal, T. W. Hansen, I. Chorkendorff, I. E. L. S. Stephens, and J. Rossmeisl, Nat. Mater. **12**, 1137 (2013).
[16] R. Ferrando, J. Jellinek, and R. L. Johnston, Chem. Rev. **108**, 845 (2008).
[17] G. Rossi, A. Rapallo, C. Mottet, A. Fortunelli, F. Baletto, and R. Ferrando, Phys. Rev. Lett. **93**, 105503 (2004).
[18] S. Lysgaard, J. S. G. Mýrdal, H. A. Hansen, and T. Vegge, Phys. Chem. Chem. Phys. **17**, 28270 (2015).
[19] B. Hartke, J. Phys. Chem. **97**, 9973 (1993).
[20] G. Rossi, R. Ferrando, A. Rapallo, A. Fortunelli, B. C. Curley, L. D. Lloyd, and R. L. Johnston, J. Chem. Phys. **122**, 194309 (2005).
[21] J. Lee, I.-H. Lee, and J. Lee, Phys. Rev. Lett. **91**, 080201 (2003).
[22] D. J. Wales and H. A. Scheraga, Science **285**, 1368 (1999).
[23] S. Goedecker, J. Chem. Phys. **120**, 9911 (2004).
[24] J. Sanchez, F. Ducastelle, and D. Gratias, Physica (Amsterdam) **128A**, 334 (1984).
[25] K. W. Jacobsen, P. Stoltze, and J. K. Nørskov, Surf. Sci. **366**, 394 (1996).
[26] G. L. Nemhauser and L. A. Wolsey, *Integer Programming and Combinatorial Optimization* (John Wiley & Sons, New York, 1988).
[27] D.-S. Chen, R. G. Batson, and Y. Dang, *Applied Integer Programming: Modeling and Solution* (John Wiley & Sons, New York, 2010).
[28] H. Wang, L. Chen, Y. Feng, and H. Chen, Acc. Chem. Res. **46**, 1636 (2013).
[29] D. Cheng, W. Wang, and S. Huang, J. Phys. Chem. B **110**, 16193 (2006).
[30] J. A. Bondy and U. S. R. Murty, *Graph Theory with Applications* (North-Holland, Amsterdam, 1976).
[31] A. M. Schoeb, T. J. Raeker, L. Yang, X. Wu, T. S. King, and A. E. DePristo, Surf. Sci. **278**, L125 (1992).
[32] S. M. Kozlov, G. Kovács, R. Ferrando, and K. M. Neyman, Chem. Sci. **6**, 3868 (2015).
[33] See Supplemental Material at http://link.aps.org/supplemental/10.1103/PhysRevLett.120.256101 for details about bonding, excited states and the C.E. model.
[34] Computational Materials Repository, https://cmr.fysik.dtu.dk/agau309/agau309.html (2017).
[35] V. Chandru and J. Hooker, *Optimization Methods for Logical Inference* (John Wiley & Sons, New York, 2011).
[36] W. Huang, D. A. Kitchaev, S. T. Dacek, Z. Rong, A. Urban, S. Cao, C. Luo, and G. Ceder, Phys. Rev. B **94**, 134424 (2016).